energies

MDPI

Article

Dynamic Wireless Power Transfer for Electric Vehicle Charging Applications: A Comparative Study of SS and LCC Compensation Topologies

Cristian Giovanni Colombo [1,*], Gabriele Bassignani [2] and Michela Longo [1]

[1] Department of Energy, Politecnico di Milano, 20156 Milan, Italy; michela.longo@polimi.it
[2] Mobility Engineering, Politecnico di Milano, 20156 Milan, Italy; gabriele.bassignani@mail.polimi.it
* Correspondence: cristiangiovanni.colombo@polimi.it

Abstract

Dynamic Wireless Power Transfer (DWPT) is attracting increasing interest as a promising solution to extend the operating range of battery electric vehicles while reducing stationary charging needs. In this study, a DWPT system for Electric Vehicle charging is investigated through a comparative simulation-based case study focused on the Italian A4 highway, a strategic transport corridor characterized by high traffic intensity and long-distance mobility demand. The proposed system is based on a segmented magnetic coupling architecture with planar circular coils installed along the roadway and a vehicle-side pickup coil. Under common roadway, vehicle, and magnetic coupling assumptions, a benchmark Tesla Model 3 Long Range traveling at a constant speed of 90 km/h and characterized by an estimated energy consumption of 0.129 kWh/km is considered. Two compensation solutions are comparatively assessed, namely the Series–Series (SS) topology and the Inductor-Capacitor-Capacitor (LCC) topology. The methodology evaluates the two topologies under the same benchmark conditions in terms of peak power, average transferred power, transferred energy per kilometer, and effect on vehicle State Of Charge (SOC). The SS topology provides a peak power of 22.52 kW, an average power of 12.30 kW, and an energy transfer of 0.14 kWh/km, whereas the LCC topology reaches a peak power of 20.44 kW, an average power of 13.47 kW, and an energy transfer of 0.15 kWh/km. Starting from an initial SOC of 30%, the final SOC after traveling through the usable electrified highway section reaches 37.48% with SS compensation and 44.28% with LCC compensation. The results show that both topologies enable effective dynamic charging, with the LCC solution exhibiting better energy transfer capability and higher operational stability, while the SS topology delivers higher instantaneous power peaks. From a comparative simulation perspective, the study supports the technical feasibility of DWPT deployment in highway environments and provides useful design insights for selecting compensation topologies in dynamic electric vehicle charging applications.

Keywords: dynamic wireless power transfer; electric vehicles; highway charging; compensation topology; SS topology; LCC topology; state of charge

Check for updates

Academic Editor: Kwok Tong Chau

Received: 6 May 2026
Revised: 30 May 2026
Accepted: 23 June 2026
Published: 24 June 2026

Copyright: © 2026 by the authors. Licensee MDPI, Basel, Switzerland. This article is an open access article distributed under the terms and conditions of the Creative Commons Attribution (CC BY) license.

1. Introduction

The rapid diffusion of Battery Electric Vehicles (BEVs) is playing a central role in the transition toward low-emission mobility systems. At the same time, fuel cell vehicles are also emerging as a relevant complementary zero-emission solution, particularly

in heavy-duty, long-haul, and high-utilization applications where fast refueling and reduced onboard battery mass may offer operational advantages [1–3]. However, despite the significant technological progress achieved in recent years, several barriers still limit the large-scale adoption of electric mobility, especially in long-distance and highway-driving applications. Among the most critical issues are limited driving range, charging downtime, infrastructure availability, and the need for increasingly large battery packs to guarantee acceptable operational autonomy [4–7]. These aspects affect both user acceptance and system-level sustainability, since larger batteries increase vehicle mass, cost, and raw material demand. In this context, Wireless Power Transfer (WPT) has emerged as a promising charging solution for electric vehicles, thanks to its capability to transfer energy without galvanic contact and with a high degree of automation [6,8]. In particular, Dynamic Wireless Power Transfer (DWPT) extends this concept by enabling energy transfer while the vehicle is in motion, thereby reducing or potentially eliminating the need for long stationary charging events. This approach may mitigate range anxiety, decrease dependence on oversized battery packs, and improve the operational flexibility of electric vehicles in high-demand transport corridors [9,10]. For these reasons, DWPT is increasingly regarded as a key enabling technology for the next generation of electrified road transport systems. The effectiveness of a DWPT system depends not only on the magnetic coupling structure, but also on the compensation topology adopted on the transmitter and receiver sides. Compensation networks are essential to improve resonant operation, increase power transfer capability, and enhance robustness against coupling variations caused by vehicle motion, vertical distance changes, and lateral misalignment [7]. Among the different solutions proposed in the literature, the Series–Series (SS) topology is generally appreciated for its simplicity, reduced component count, and high peak power capability, while the Inductor–Capacitor–Capacitor (LCC) topology is often preferred for its higher stability, current controllability, and improved resilience to operating variations [11–13]. Therefore, the comparison between these two topologies is particularly relevant in dynamic charging applications, where mutual inductance continuously changes during vehicle travel [14]. Although several studies have investigated WPT and DWPT systems from electrical, electromagnetic, and control perspectives, fewer contributions directly connect compensation topology performance with a realistic highway deployment scenario and its actual effect on vehicle energy balance over long travel distances [15–17]. In particular, infrastructure-oriented case studies that combine road context, vehicle benchmark, compensation network analysis, and State Of Charge (SOC) evolution are still limited. This aspect is especially important for assessing the practical relevance of DWPT solutions beyond component-level or laboratory-scale evaluations. From a literature-structuring perspective, existing contributions can be broadly grouped into three categories. A first group mainly addresses resonant compensation design and circuit-level power transfer behavior, often with emphasis on topology analysis under idealized coupling conditions [7,14]. A second group focuses on electromagnetic coupling, control strategies, and local dynamic-operating behavior, including sensitivity to alignment and operating variations [7,18]. A third and more limited group considers application-oriented DWPT scenarios, in which electrical performance is examined together with vehicle energy demand, roadway deployment assumptions, and charging outcomes over distance [14,19]. It is within this third category that a clearer research need still emerges, namely the development of comparative topology studies that explicitly connect SS/LCC performance with highway-oriented infrastructure conditions and vehicle-level SOC implications. Starting from this research gap, this paper investigates the feasibility of a DWPT charging system for electric vehicles through a real-world-inspired case study focused on the Italian A4 highway. The A4 corridor represents one of the most strategically relevant road axes in Italy, connecting major industrial and

commercial areas and supporting intense daily traffic flows. Within this framework, a segmented DWPT architecture based on planar circular coils is considered, and two alternative compensation solutions are comparatively analyzed: the SS topology and the LCC topology. The study adopts a benchmark BEV traveling at constant highway speed, and evaluates the system in terms of transferred power, transferred energy, and impact on the vehicle SOC. The main contribution of this work is threefold:

1. It proposes a realistic DWPT application scenario for a major highway corridor, linking infrastructure characteristics and electric vehicle charging requirements;
2. It provides a comparative assessment of SS and LCC compensation topologies under the same magnetic and dynamic assumptions, highlighting the trade-off between peak power capability and energy transfer stability;
3. It connects the electrical behavior of the DWPT system to the vehicle-level charging outcome, thus providing a more application-oriented interpretation of topology performance.

In this way, the paper aims to support the design and selection of compensation solutions for future highway-based dynamic charging infrastructures. The main contribution of this work lies in integrating the topology comparison into a highway-oriented, infrastructure-referenced, and vehicle-level assessment framework, in which circuit behavior is directly linked to transferred energy and SOC evolution over a realistic long-distance operating scenario. The remainder of the paper is organized as follows. Section 2 presents the selected highway scenario and summarizes the main case study assumptions. Section 3 describes the DWPT system architecture and the adopted magnetic configuration. Section 4 discusses the benchmark vehicle and the corresponding energy demand target for dynamic charging. Section 5 introduces the modeling approach, the investigated compensation topologies, and the main simulation assumptions. Section 6 presents the simulation results in terms of power transfer, energy performance, and SOC evolution. Section 7 discusses the main implications of the findings for highway DWPT design. Finally, Section 8 summarizes the main conclusions and outlines future research directions.

2. Case Study and Highway Scenario

To assess the practical applicability of DWPT for highway BEV charging, a real-world-inspired case study was developed by considering the Italian A4 highway as the reference infrastructure. This corridor was selected because of its strategic relevance within the national and European transport network, its high traffic density, and its role in connecting major industrial and commercial areas across Northern Italy. As such, the A4 highway represents a suitable environment for evaluating the potential of dynamic charging systems in long-distance mobility applications [20,21]. The overall length of the considered highway stretch is approximately 523 km, extending from Turin to Trieste. However, due to technical and installation-related constraints, the section assumed to be effectively suitable for DWPT deployment was limited to 510 km. This distinction is important, since the feasibility of large-scale dynamic charging infrastructure depends not only on electrical performance, but also on roadway characteristics, equipment integration requirements, and the availability of usable road segments. Another relevant factor supporting the selection of the A4 highway is its high traffic intensity. The corridor is reported to accommodate approximately 108,000 vehicles per day, which makes it one of the busiest highway systems in Italy. Moreover, the A4 axis plays a key role in freight and passenger mobility and is part of the broader trans-European transport framework. These features make it particularly meaningful as a reference case for evaluating whether a DWPT system could provide tangible benefits in terms of charging support for battery electric vehicles operating under sustained highway conditions. From an infrastructural standpoint, the selected scenario is

also appropriate because large portions of the highway are characterized by a relatively regular layout, with three lanes per driving direction in many sections. This feature is relevant when discussing the possible integration of segmented transmitter coils within the roadway and the overall scalability of the charging architecture. In the present study, the highway context is therefore not treated as an abstract mobility scenario, but as a realistic application domain in which infrastructure, vehicle energy demand, and DWPT system behavior can be jointly analyzed. Table 1 highlights the case study and the main vehicle assumptions.

Table 1. Case study and benchmark vehicle assumptions.

Parameter	Value	Unit
Highway corridor	A4 (Turin–Trieste)	–
Total route length	523	km
Electrifiable/usable DWPT length	510	km
Traffic volume	108,000	vehicles/day
Typical highway layout	3 lanes per direction	–
Reference vehicle	Tesla Model 3 Long Range	–
Battery capacity	75	kWh
Cruising speed	90 (25)	km/h (m/s)
Initial SOC in baseline benchmark	80	%
Recharge threshold SOC	10	%
Average energy consumption	0.129	kWh/km

The main numerical assumptions related to the highway scenario and benchmark vehicle are summarized in Table 1. These values define the reference application context adopted throughout the paper, including the route length, traffic relevance, vehicle class, and baseline energy demand conditions. The energetic implications of the benchmark vehicle, and in particular the role of the 0.129 kWh/km consumption value as the reference target for DWPT performance assessment, are discussed in detail in Section 4. Within this application framework, the analysis is intentionally developed by adopting a single benchmark EV as the reference charging subject. This assumption provides a controlled basis for evaluating the electrical and energetic behavior of the DWPT system before introducing the additional complexity associated with simultaneous multi-vehicle operation.

3. DWPT System Architecture

The DWPT system considered in this study is based on a segmented primary-side architecture for electric vehicle charging during motion. In this configuration, the transmitting side is integrated into the roadway through a sequence of discrete ground-embedded coils, while the receiving side is installed underneath the vehicle. Energy transfer is achieved through magnetic coupling between the road-side transmitter coil and the vehicle-side pickup coil as the vehicle travels along the electrified highway segment. This segmented layout is particularly suitable for highway DWPT applications because it distributes the charging infrastructure along the roadway while avoiding unnecessary energization of the full road section. In practical terms, only the coils interacting with the vehicle need to operate during transit, which improves conceptual scalability and supports a more realistic infrastructure-oriented implementation. From the electromagnetic point of view, the proposed DWPT system employs planar circular coils on both the transmitter and receiver sides. This choice was made because circular coils provide a relatively symmetric magnetic field distribution, low geometric complexity, and improved tolerance to angular misalignment when compared with more irregular layouts. They are also attractive from an implementation perspective because of their simpler construction and reduced magnetic

field concentration at sharp edges [22–24]. The transmitter coil adopted in the present study has a diameter of 1 m and consists of 28 turns, while the receiver coil has a diameter of 0.4 m and consists of 24 turns. Equivalently, the same geometry can be described by considering radii of 0.5 m and 0.2 m for the primary and secondary sides, respectively. This size difference reflects the different functional roles of the two elements: the road-side coil is designed to generate a magnetic field over a broader interaction area, whereas the vehicle-side coil is constrained by packaging requirements and underbody installation limits. The ground-side deployment strategy was defined by assuming 250 transmitting coils per kilometer of electrified roadway. This value corresponds to a repeated segmented arrangement in which adjacent active coil zones are separated by intermediate spaces of approximately 3 m. These inter-coil gaps are intended to accommodate auxiliary infrastructure elements such as cabling, sensors, power electronics connections, monitoring devices, and other installation-related components. Such a layout is consistent with the practical need to avoid continuous coil occupation of the full road surface and to preserve a feasible spacing for field infrastructure integration. Table 2 collects the main assumptions for DWPT architectures and coils parameters, and Figure 1 presents the layout of the system. It should be noted that the adopted roadway deployment density also has direct implications for infrastructure cost, installation effort, and maintenance requirements. In the present work, however, this parameter is introduced primarily to define a consistent technical comparison framework for the investigated compensation topologies, rather than to provide a full techno-economic optimization of the DWPT infrastructure.

Table 2. DWPT architecture and roadway deployment parameters.

Parameter	Value	Unit
Primary coil geometry	Planar circular coil	–
Secondary coil geometry	Planar circular coil	–
Primary coil diameter	1.0	m
Secondary coil diameter	0.4	m
Primary coil radius	0.5	m
Secondary coil radius	0.2	m
Primary turns	28	–
Secondary turns	24	–
Roadway architecture	Segmented primary-side layout	–
Transmitter coils per kilometer	250	coils/km
Inter-coil spacing	3	m

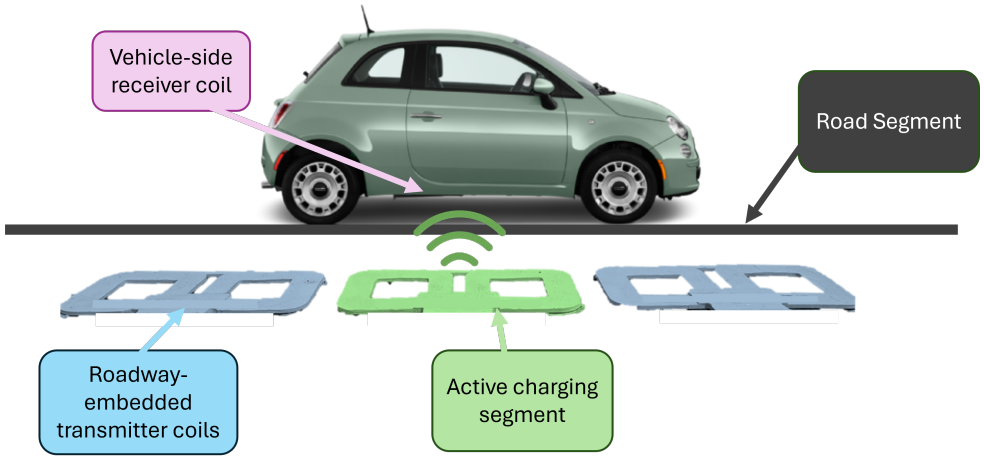


Figure 1. Conceptual layout of the segmented DWPT system considered in this work, showing roadway-embedded transmitter coils, vehicle-side pickup coil, and the repeated deployment of active charging segments along the highway.

Under this arrangement, the DWPT roadway behaves as a sequence of localized magnetic interaction regions. As the vehicle advances at constant speed, the receiver coil experiences a time-varying coupling condition with each energized transmitter segment. Consequently, the transferred power is not spatially uniform, but evolves according to the relative position between the transmitter and receiver coils. This aspect is fundamental for interpreting the power and energy results presented later in the paper, since the instantaneous charging performance depends on coil overlap and on the associated variation in mutual inductance. By keeping unchanged the coil dimensions, roadway segmentation, and vehicle-motion scenario, the proposed architecture provides a consistent physical basis for comparing the two compensation topologies under identical geometric and infrastructural assumptions. Overall, the segmented road-side installation, planar circular coil geometry, and selected transmitter–receiver sizing define the physical framework within which the two investigated compensation solutions can be meaningfully assessed. The next section therefore introduces the vehicle benchmark and the energy demand analysis used to quantify the charging requirement that the DWPT system is expected to satisfy.

4. Vehicle Benchmark and Energy Demand

The main vehicle and driving assumptions adopted in this study are summarized in Table 1. On the basis of these assumptions, a baseline non-DWPT drive-cycle benchmark was used to determine the energetic target that the proposed charging infrastructure must satisfy during highway operation [25–27]. In this respect, the adopted 90 km/h operating condition should be interpreted as a controlled highway benchmark rather than as a full representation of real traffic behavior. The purpose of this assumption is to define a consistent reference condition for comparing the investigated compensation topologies, while avoiding additional variability associated with acceleration phases, speed fluctuations, congestion, and lane changes. For the selected Tesla Model 3 Long Range benchmark, constant-speed travel at 90 km/h over the A4 route yields an average energy consumption of 0.129 kWh/km. In the context of this study, this value is the key design reference because it represents the minimum energy that the DWPT system should transfer per traveled kilometer in order to compensate for battery depletion during motion. Accordingly, the comparison between the vehicle consumption and the energy transferred by the roadway infrastructure provides the most direct criterion for assessing the usefulness of the proposed dynamic charging system. If the transferred energy is lower than 0.129 kWh/km, the vehicle battery will continue to discharge, even though at a slower rate than in the no-charging case. If, by contrast, the transferred energy exceeds this threshold, the DWPT system will not only sustain vehicle operation but will also produce a net charging effect during motion. This interpretation is central to the comparative analysis carried out in the remainder of the paper, because it links topology-level electrical performance directly to vehicle-level charging outcome. The baseline benchmark also indicates that, under the adopted constant-speed assumptions, a conventional trip without dynamic charging would require a stationary recharge stop before the completion of the full A4 route [21,27]. This observation further motivates the investigation of DWPT as an enabling technology for long-distance electric mobility and justifies the use of the benchmark-consumption value as the reference energetic target throughout the results and discussion sections. The following section therefore introduces the adopted modeling approach and the two compensation topologies investigated in this study, namely the SS and the LCC configurations.

5. Compensation Topologies and Modeling

This section introduces the electrical modeling framework adopted to compare the two compensation solutions considered in this work, namely the SS and the LCC topologies.

More specifically, the methodology consists of a comparative simulation-based assessment in which the two compensation topologies are evaluated under the same benchmark vehicle, roadway deployment, operating frequency, and magnetic coupling assumptions. The analytical procedure combines a position-dependent coupling model, topology-specific resonant circuit formulations, and vehicle-level energy balance interpretation in order to compare transferred power, transferred energy, and SOC evolution within a common application-oriented framework. The comparison is carried out under the same vehicle, roadway, and magnetic coupling assumptions, so that the impact of the compensation network on the overall DWPT performance can be assessed in a consistent manner. Figure 2 presents the workflow adopted in this case study.

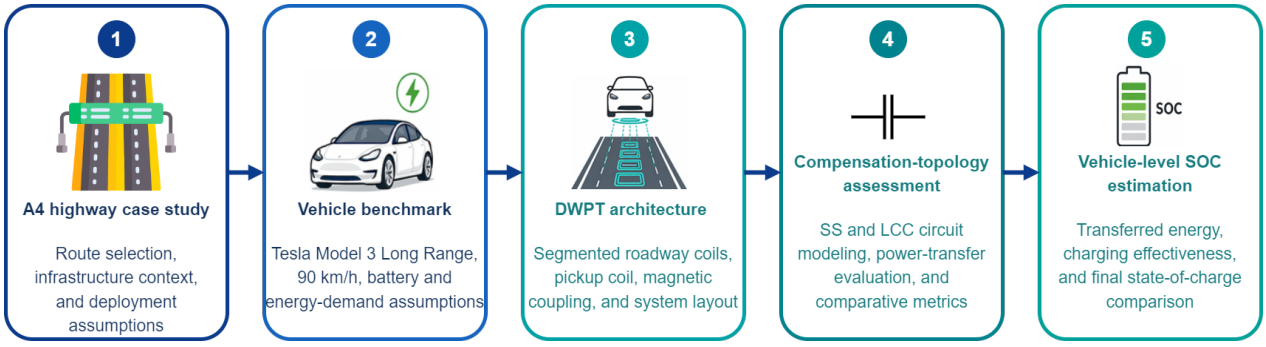


Figure 2. Workflow adopted in the study, from highway case definition and vehicle benchmark to DWPT architecture modeling, compensation topology assessment, and vehicle-level SOC evaluation.

The electrical parameters of the compensation networks were selected according to standard WPT design criteria to ensure resonance at the operating frequency.

5.1. Modeling Framework

The proposed DWPT system is analyzed by considering the dynamic interaction between the segmented primary coils embedded in the roadway and the pickup coil installed underneath the vehicle. As the vehicle moves along the electrified highway section, the relative position between transmitter and receiver changes continuously, resulting in a time-varying magnetic coupling condition. Consequently, the mutual inductance is not constant, but varies during motion according to the instantaneous alignment between the two coils.

For consistency with the adopted theoretical formulation, the mutual inductance is first expressed as (1), where M is the mutual inductance, k is the coupling coefficient, and L_p and L_s are the self-inductances of the primary and secondary coils, respectively.

$$M = k\sqrt{L_p L_s} \tag{1}$$

In the dynamic charging scenario considered in this paper, the mutual inductance must be interpreted as a position-dependent quantity, $M = M(x)$, where x denotes the instantaneous longitudinal position of the vehicle with respect to the active roadway segment. To provide a more physically meaningful representation of the coupling variation, the coupling coefficient is modeled as a function of position following (2), where $k_{\max}$ represents the maximum coupling under optimal alignment conditions and d is a characteristic distance related to the coil geometry.

$$k(x) = k_{\max} \cdot \frac{1}{1 + \left(\frac{x}{d}\right)^2} \tag{2}$$

This formulation captures the decay of magnetic coupling due to longitudinal misalignment and finite coil dimensions, consistently with established inductive power transfer models [22]. Accordingly, all current, power, and energy quantities derived in the following subsections are also position-dependent, even when this dependence is omitted for compactness of notation.

For the additional sensitivity analysis introduced later in the paper, a normalized coupling-reduction factor, denoted by $\alpha \in (0, 1]$, is also considered. In this formulation, $\alpha = 1$ represents the nominal alignment condition, whereas $\alpha < 1$ represents degraded coupling conditions associated with dynamic displacement, lateral misalignment, or other geometric deviations from the ideal operating point. Accordingly, the mutual inductance used in the sensitivity analysis is expressed as (3).

$$M_\alpha(x) = \alpha M(x) \tag{3}$$

This definition is not intended to replace a full geometric misalignment model. Rather, it provides a compact and physically interpretable parameterization for evaluating the robustness of the investigated compensation topologies under reduced-coupling conditions [28]. In this sense, the factor α should be interpreted as an aggregate sensitivity parameter that compactly represents the overall reduction of magnetic coupling caused by non-ideal operating conditions. These may include, among others, lateral misalignment, vertical air gap variation, and geometric or installation tolerances. In practical motorway operation, such vertical air-gap variation may also originate from suspension-induced oscillations and other transient vehicle body motions. Since magnetic coupling is highly sensitive to the transmitter–receiver spacing, these effects may alter the instantaneous transferred power and the effective cumulative energy delivered during motion. However, the present formulation does not resolve the individual contribution of each of these effects separately. More specifically, the present formulation should be interpreted as a reduced-order system-level model intended for comparative topology assessment. As such, it captures the longitudinal evolution of the coupling condition in a computationally efficient way, but it does not explicitly resolve lateral misalignment, vertical displacement variations, or vehicle pitch/roll effects. These aspects are recognized as relevant to real-world DWPT behavior and are identified as an important direction for future model refinement.

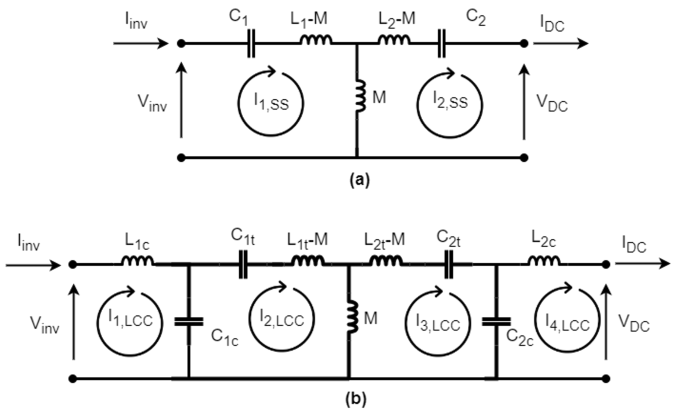
The transferred power is evaluated over the vehicle transit interval and then used to estimate the delivered energy. In general terms, the energy transferred by the DWPT system is computed through (4), where $P_{\text{out}}(t)$ is the instantaneous output power and the factor $1/3600$ converts the result into kWh when power is expressed in kW and time in seconds.

$$E_{\text{tr}} = \frac{1}{3600} \int_{t_{\text{start}}}^{t_{\text{end}}} P_{\text{out}}(t)\, dt \tag{4}$$

This formulation is particularly suitable for DWPT applications because it allows the charging capability of the infrastructure to be assessed not only in terms of instantaneous power peaks, but also in terms of effective energy supplied to the vehicle over distance.

Based on this framework, the two compensation topologies are compared using the following key performance indicators: peak output power, average output power, transferred energy per kilometer, and final battery SOC. These metrics allow both the electrical behavior of the resonant networks and their practical impact on vehicle charging performance to be evaluated within the same application-oriented perspective.

Figure 3 proposes the graphical representations of the two compensation topologies analyzed for the performance study.



Symbol	Description
I_{inv}	Inverter-side input current
V_{inv}	Inverter-side input voltage
I_{dc}	DC-side output current
V_{dc}	DC-side output voltage
C_1	Primary-side series capacitor in the SS topology
C_2	Secondary-side series capacitor in the SS topology
L_1-M	Primary-side leakage inductance in the SS topology
L_2-M	Secondary-side leakage inductance in the SS topology
M	Mutual inductance between primary and secondary coils
$I_{1,SS}$	Primary loop current in the SS topology
$I_{2,SS}$	Secondary loop current in the SS topology
L_{1c}	Input-side series inductor in the LCC topology
C_{1c}	Input-side shunt capacitor in the LCC topology
C_{1t}	Primary-side series capacitor in the LCC topology
L_{1t}-M	Primary-side leakage inductance in the LCC topology
L_{2t}-M	Secondary-side leakage inductance in the LCC topology
C_{2t}	Secondary-side series capacitor in the LCC topology
C_{2C}	Output-side shunt capacitor in the LCC topology
L_{2C}	Output-side series inductor in the LCC topology
$I_{1,LCC}$	Input loop current in the LCC topology
$I_{2,LCC}$	Primary resonant loop current in the LCC topology
$I_{3,LCC}$	Secondary resonant loop current in the LCC topology
$I_{4,LCC}$	Output loop current in the LCC topology

Figure 3. Compensation networks considered in this study: (**a**) SS topology, and (**b**) LCC topology.

5.2. Series–Series Compensation Topology

The SS topology represents one of the simplest and most established compensation solutions for wireless power transfer systems. In this configuration, both the primary and secondary coils are compensated by series capacitors, so that the inductive reactances are balanced at the operating angular frequency ω_0.

Under tuned resonant conditions, the SS topology can be described using a reflected-impedance formulation in which the primary and secondary loop currents are directly related through the mutual inductance. In particular, the primary-side current can be expressed as (5), where V_{inv} is the inverter-side voltage, R_p and R_s are the primary- and secondary-side equivalent resistances, R_L is the equivalent load resistance, and $M(x)$ is the position-dependent mutual inductance.

$$I_{1,\text{SS}}(x) = \frac{V_{\text{inv}}}{R_p + \dfrac{\omega_0^2 M(x)^2}{R_s + R_L}} \tag{5}$$

The corresponding secondary-side loop current is then written as (6).

$$I_{2,\text{SS}}(x) = \frac{j\omega_0 M(x)}{R_s + R_L} I_{1,\text{SS}}(x) \tag{6}$$

Accordingly, the output power of the SS topology is evaluated as (7), where η is the overall transfer efficiency.

$$P_{\text{out,SS}}(x) = \eta |I_{2,\text{SS}}(x)|^2 R_L \tag{7}$$

This formulation highlights that the SS power profile is strongly driven by the variation of $M(x)$ along the roadway. As a result, the topology exhibits pronounced power peaks under favorable alignment conditions and reduced transfer capability when the coupling decreases. This behavior makes the SS topology suitable for applications requiring high instantaneous power, but more sensitive to coupling variations in dynamic charging scenarios [28]. Moreover, this formulation is intended to describe the SS topology under nominal resonant operation within the comparative framework adopted in this study. It should not be interpreted as a complete representation of off-resonance or detuned operat-

ing conditions, under which the loop currents, transferred power, and effective charging performance may deviate from the values predicted by the tuned model.

5.3. Inductor–Capacitor–Capacitor Compensation Topology

The LCC topology is a multi-resonant compensation solution designed to provide improved current controllability and reduced sensitivity to coupling and load variations. In DWPT applications, this topology is particularly attractive because it can sustain a more stable primary current under dynamic operating conditions.

Under resonant conditions, the LCC topology can be interpreted as a current-source-like network. More precisely, this behavior is obtained under tuned operation, assuming appropriate compensation design and operating conditions such as zero-phase-angle behavior or equivalent resonant control objectives. In the present study, the LCC formulation is therefore adopted in simplified resonant form and is intended to represent the intrinsic topology behavior under idealized tuning assumptions, rather than a fully control-resolved implementation model. Accordingly, the primary-side current is primarily determined by the compensation inductance and can be expressed as (8), where $L_{\mathrm{eq}} = L_{1c} + L_p$ represents the equivalent input inductance. This expression holds under tuned resonant conditions, assuming suitable operating-point regulation and proper selection of the compensation components.

$$I_{1,\mathrm{LCC}} = \frac{V_{\mathrm{inv}}}{\omega_0 L_{\mathrm{eq}}} \tag{8}$$

Thus, the output-side current is related to the mutual inductance and compensation capacitors as (9).

$$I_{4,\mathrm{LCC}}(x) = -j\omega_0^3 C_{pc} C_{sc} M(x) V_{\mathrm{inv}} \tag{9}$$

Then, the corresponding output power is computed by (10).

$$P_{\mathrm{out,LCC}}(x) = |I_{4,\mathrm{LCC}}(x)| V_{\mathrm{DC}} \tag{10}$$

Under these conditions, the LCC topology behaves as a controlled current source, significantly reducing its dependence on variations in $M(x)$ [11–13]. As a consequence, the power transfer profile is smoother and more uniform along the roadway, leading to improved cumulative energy transfer in dynamic charging applications. This characteristic makes the LCC topology particularly suitable when the objective is to maximize the effective energy delivered to the vehicle rather than the instantaneous peak power. These formulations provide the basis for the comparative analysis presented in the following section.

5.4. Comparative Assessment Criteria

To ensure a fair comparison, both compensation topologies are evaluated under the same roadway scenario, vehicle benchmark, and coil geometry described in the previous sections. The comparison is not limited to a purely electrical viewpoint, but explicitly includes the charging implications at vehicle level. In particular, the transferred energy per kilometer is compared against the benchmark vehicle demand of 0.129 kWh/km in order to determine whether the DWPT system is able to merely reduce battery depletion or to produce a net recharge effect during motion. Accordingly, the subsequent results section is structured around four complementary indicators: the peak power, which captures the maximum transfer capability of the system; the average power, which reflects the overall stability of the charging process; the transferred energy per kilometer, which directly quantifies infrastructure usefulness; and the final SOC, which provides the most immediate vehicle-level interpretation of DWPT performance. This approach allows the technical differences between SS and LCC compensation to be translated into design-oriented conclu-

sions for highway dynamic charging applications. The present comparison is not intended to represent two independently globally optimized compensation networks obtained under different design objectives. Rather, the SS and LCC topologies were configured under a common comparative framework, based on the same operating frequency, roadway scenario, vehicle benchmark, coil geometry, and coupling assumptions, so that the observed differences can be interpreted primarily in relation to topology behavior under consistent tuned conditions.

5.5. Simulation Assumptions

To improve reproducibility and make the methodological framework more explicit, the main simulation assumptions adopted throughout the comparative study are summarized here. All simulations were carried out under the same highway scenario, vehicle benchmark, coil geometry, and roadway segmentation described in Tables 1 and 2, so that the observed performance differences can be attributed to the adopted compensation topology rather than to changes in external conditions. Following this approach, the electrical parameter settings of the two compensation networks were selected to ensure resonant operation and fair comparability under the same benchmark conditions, rather than to maximize each topology independently under topology-specific objective functions. Therefore, the present results should be interpreted as a tuned comparative assessment under aligned design assumptions. Table 3 summarizes the main electrical, geometric, and vehicle-side assumptions adopted in the comparative DWPT model.

Table 3. Electrical and simulation parameters adopted in the comparative DWPT model.

Parameter	Value	Unit
Resonant frequency, f_0	85	kHz
Angular frequency, $\omega_0 = 2\pi f_0$	5.34×10^5	rad/s
Vehicle speed, v	90 (25)	km/h (m/s)
Usable DWPT route length	510	km
Battery capacity	75	kWh
Battery-side DC voltage, V_{DC}	400	V
Inverter-side voltage, V_{inv}	500	V
Overall efficiency, η	0.90	–
Primary coil radius, r_p	0.5	m
Secondary coil radius, r_s	0.2	m
Primary turns, N_p	28	–
Secondary turns, N_s	24	–
Transmitter coils per kilometer	250	coils/km
Inter-coil spacing	3	m
Initial SOC for comparative assessment	30	%
Benchmark energy demand	0.129	kWh/km
Transferred energy (SS)	0.14	kWh/km
Transferred energy (LCC)	0.15	kWh/km
Peak power (SS)	22.52	kW
Peak power (LCC)	20.44	kW
Average power (SS)	12.30	kW
Average power (LCC)	13.47	kW

From the vehicle and route standpoint, the benchmark battery electric vehicle was modeled with a battery capacity of 75 kWh and a constant cruising speed of 90 km/h (25 m/s) over the 523 km A4 route, of which 510 km were considered effectively suitable for DWPT deployment. In the baseline non-DWPT benchmark, the initial SOC was set to 80% and the conventional recharge threshold to 10%. For the comparative charging assessment presented in Section 6, the vehicle was assumed to enter the electrified route with an initial

SOC of 30%. From the electrical standpoint, the LCC-based formulation was evaluated using an inverter-side voltage of 500 V and a battery-side voltage of 400 V, consistent with the circuit expressions introduced. For the SS-based formulation, the overall transfer efficiency was assumed equal to $\eta = 0.9$. In the present study, this efficiency term is introduced as a lumped system-level parameter to support a controlled comparative assessment under identical operating assumptions. Accordingly, it should not be interpreted as a temperature-dependent or load-dependent electro-thermal efficiency model. The operating frequency was fixed at the resonant design value adopted in the circuit models, denoted as f_0 in frequency form or $\omega_0 = 2\pi f_0$ in angular form. Finally, all comparative simulations were performed by keeping constant the transmitter–receiver geometry, roadway segmentation, and vehicle speed, while allowing the magnetic coupling condition to vary with the relative coil position. This assumption is consistent with the dynamic nature of the proposed DWPT application and ensures that the comparison between SS and LCC topologies is carried out under identical operating conditions. Accordingly, the reported power, energy, and SOC results should be interpreted as reference comparative outcomes under idealized constant-speed highway operation. Within this framework, sensitivity to the coupling condition is partially explored through the normalized reduction factor α, whereas vehicle speed and roadway coil spacing are treated as fixed benchmark parameters in the present study. Therefore, the current analysis should be interpreted as a topology-comparison framework under aligned operating assumptions rather than as a full multi-parameter sensitivity study. In real traffic conditions, acceleration, deceleration, lane changes, and congestion may modify both the duration and regularity of the coupling intervals, thereby affecting the average transferred energy and the final SOC evolution.

6. Results

This section presents the simulation results obtained for the two compensation topologies considered in this study, namely the SS and the LCC configurations. The results are discussed with reference to the main performance indicators introduced in the previous section: peak power, average power, transferred energy per kilometer, and effect on vehicle SOC. The comparison is performed under the same roadway, vehicle, and magnetic coupling assumptions in order to isolate the influence of the compensation network on the DWPT performance.

6.1. Results for the Series–Series Topology

The observed power oscillations are directly related to the spatial variation of the mutual inductance M(x), which governs the instantaneous coupling between the transmitter and receiver coils. The SS compensation topology showed the highest instantaneous power capability among the two examined solutions. Under the adopted operating conditions, the maximum transferred power reached 22.52 kW, while the average transferred power was equal to 12.30 kW. The corresponding transferred energy was 0.14 kWh/km. These values indicate that the SS network is capable of providing substantial power peaks when the alignment condition between the transmitter and receiver coils is favorable. This behavior is consistent with the expected operating characteristics of the SS topology, which tends to concentrate the energy transfer capability in localized intervals of strong magnetic coupling. As a result, the power profile is characterized by a pronounced variation along the vehicle trajectory, with high transfer peaks and more limited charging performance outside the optimal interaction region. From the energetic viewpoint, the transferred energy per kilometer is greater than the benchmark vehicle demand of 0.129 kWh/km introduced in the previous section. Therefore, even though the SS topology exhibits a less uniform power profile, the obtained result already suggests that this configuration is capable of

supporting not only compensation of the vehicle consumption, but also a net charging contribution during motion.

6.2. Results for the LCC Topology

The LCC compensation topology exhibited a different behavior, characterized by a slightly lower peak power but a higher average power and a larger transferred energy over distance. In the considered case, the maximum transferred power reached 20.44 kW, whereas the average transferred power increased to 13.47 kW. The resulting energy transferred to the vehicle was equal to 0.15 kWh/km. Although the peak value is lower than that obtained with the SS configuration, the LCC topology demonstrated a more stable transfer process over the interaction interval. This result is reflected by the higher average power and by the increased energy delivered per kilometer. Such an outcome is coherent with the expected behavior of the LCC network, whose compensation structure allows a more robust response to coupling variations and a less pronounced dependence on the instantaneous alignment condition. From the application perspective, the LCC results are particularly relevant because dynamic charging effectiveness is not determined solely by the highest instantaneous power value, but by the capability to sustain energy transfer over time and distance. In this sense, the LCC solution appears more effective in exploiting the available interaction interval between road-side and vehicle-side coils.

6.3. Comparative Performance Assessment

To provide a compact representation of result sensitivity under non-ideal coupling conditions, the revised figures include variation ranges obtained by introducing moderate perturbations of the normalized coupling factor around the nominal case ($\alpha = 1$). In particular, $\alpha = 0.95$, 0.975, and 1 were considered. Figure 4 presents a comparative representation of the output power profiles of the two compensation topologies over the first 100 m. The SS configuration exhibits higher instantaneous power peaks, whereas the LCC topology provides a flatter and more regular transfer profile. This more regular behavior is quantitatively reflected by the higher average transferred power of the LCC topology, 13.47 kW with respect to 12.30 kW for SS, its larger transferred energy per kilometer, 0.15 kWh/km with respect to 0.14 kWh/km, and its stronger vehicle-level charging outcome in terms of final SOC.

On the other hand, Figure 5 presents the comparative analysis of the transferred energy over 100 m for the two analyzed compensation topologies. Despite the lower peak power, the LCC topology achieves a higher cumulative energy transfer due to its more stable power delivery profile.

A direct comparison between the two topologies highlights a clear trade-off between peak power capability and energy transfer stability. The SS topology achieved the highest peak power, with 22.52 kW versus 20.44 kW for the LCC topology. However, the LCC configuration provided both a higher average power and a higher transferred energy per kilometer, with values of 13.47 kW and 0.15 kWh/km, respectively, compared with 12.30 kW and 0.14 kWh/km for the SS solution. In these two figures, the central curve corresponds to the nominal operating condition, whereas the shaded bands and variation ranges indicate the sensitivity of the results to moderate coupling fluctuations around the nominal case. This representation is intended to provide not only the nominal comparative trend, but also a compact visual indication of result robustness under non-ideal operating conditions. Although the absolute difference in average power may appear moderate, the practical relevance becomes more evident when interpreted over the full usable DWPT-equipped route. In particular, the higher transferred energy of the LCC topology accumulates over distance and produces a stronger vehicle-level charging effect, which is reflected in the

larger final SOC increase reported later in the paper. By contrast, the higher peak power of the SS topology mainly reflects stronger instantaneous transfer capability under favorable alignment conditions, but does not translate into the highest cumulative charging benefit. Table 4 offers a comprehensive performances comparison between the two compensation topologies in the analyzed case study.

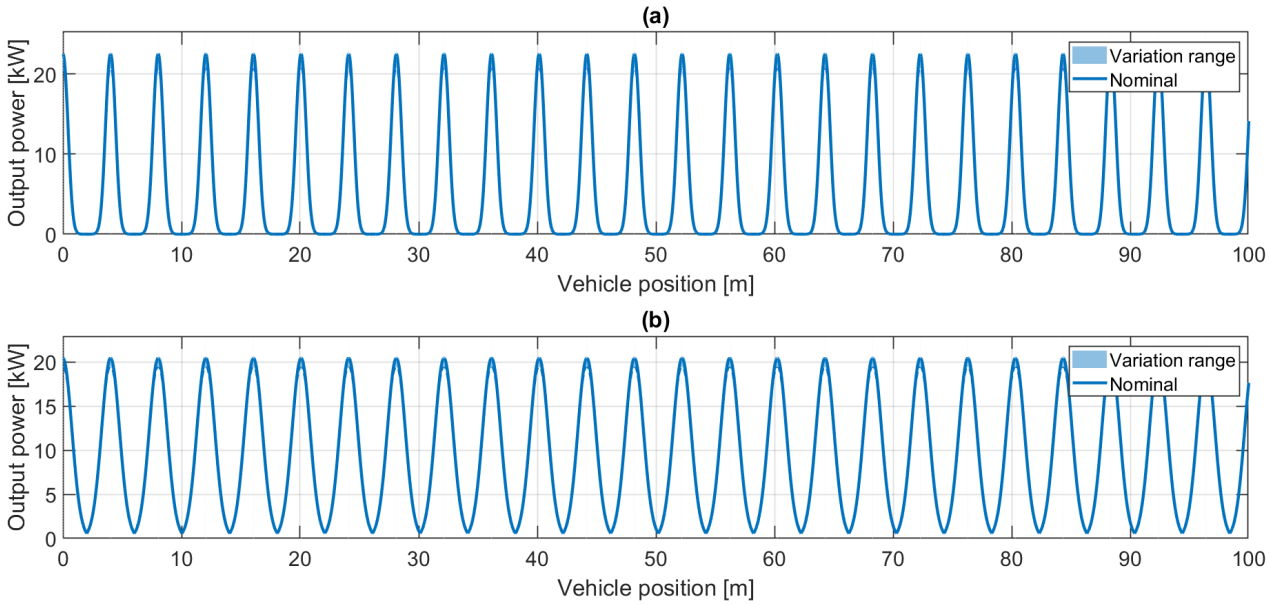


Figure 4. Output power profiles over the first 100 m of electrified roadway for the two investigated compensation topologies, including variation ranges derived from moderate coupling fluctuations around the nominal operating condition: (**a**) SS compensation topology, (**b**) LCC compensation topology.

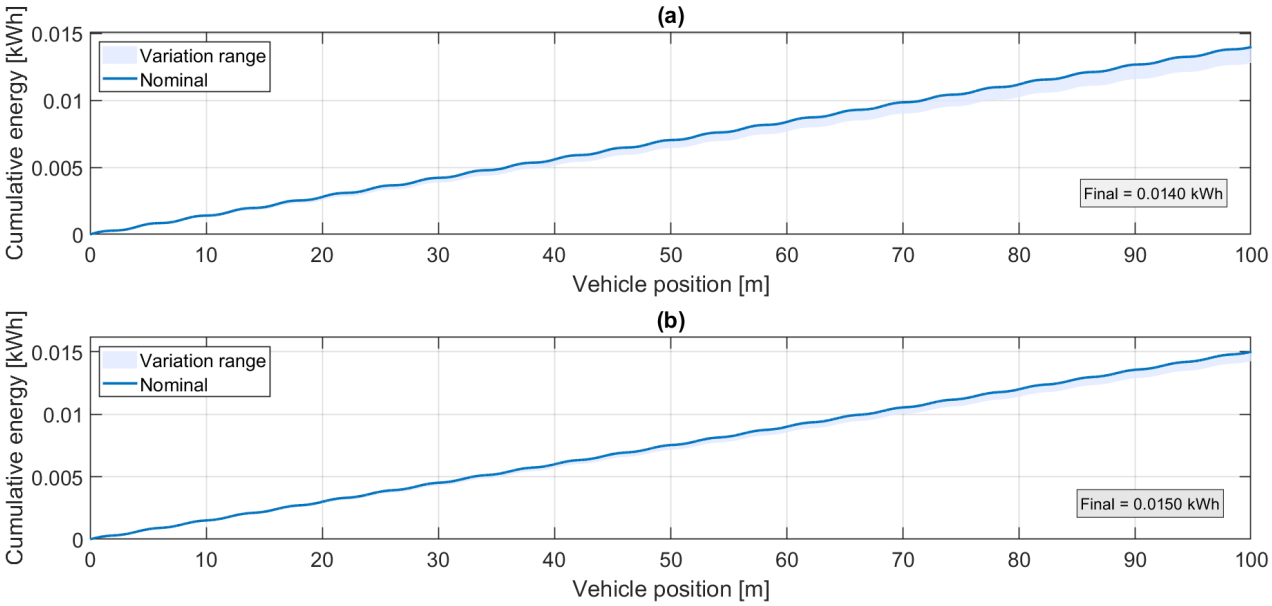


Figure 5. Cumulative transferred energy over the first 100 m of electrified roadway for the two investigated compensation topologies, including variation ranges derived from moderate coupling fluctuations around the nominal operating condition: (**a**) SS topology, (**b**) LCC topology.

Table 4. Comparative performance of SS and LCC compensation topologies.

Metric	SS	LCC
Peak power (kW)	22.52	20.44
Average power (kW)	12.30	13.47
Transferred energy (kWh/km)	0.14	0.15
Initial SOC (%)	30.00	30.00
Final SOC (%)	37.48	44.28
SOC increase (percentage points)	7.48	14.28

These results show that the topology offering the highest instantaneous power is not necessarily the one ensuring the best overall charging effectiveness in a dynamic scenario. In highway DWPT operation, where the magnetic coupling changes continuously as the vehicle moves, the regularity of the power transfer process becomes at least as important as the absolute peak value. Consequently, the wider and flatter power profile associated with the LCC topology leads to a more favorable energy transfer outcome over the traveled distance. The comparison therefore suggests that the SS topology is more suitable when a simpler and potentially lower-cost architecture is desired, particularly in applications where high instantaneous power is a priority. By contrast, the LCC topology appears more advantageous when the objective is to maximize the useful energy supplied to the vehicle under variable dynamic operating conditions.

6.4. Effect on Vehicle State of Charge

To evaluate the practical impact of the DWPT system on vehicle operation, the transferred energy was translated into battery state-of-charge evolution over the equipped highway section. In this analysis, the vehicle was assumed to enter the electrified route with an initial SOC of 30%, representing a realistic condition in which charging support is needed during the trip. Figure 6 presents the corresponding SOC comparison for the SS and LCC compensation topologies, while Figure 7 illustrates the corresponding net energy balance over the usable DWPT-equipped route.

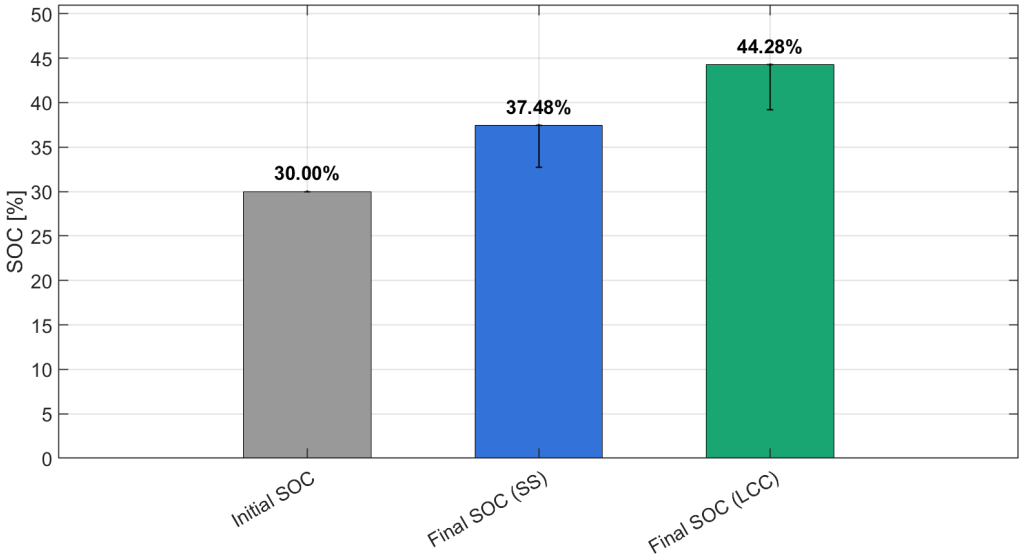


Figure 6. Vehicle SOC comparison for the two investigated compensation topologies, including variation ranges derived from moderate coupling fluctuations around the nominal operating condition.

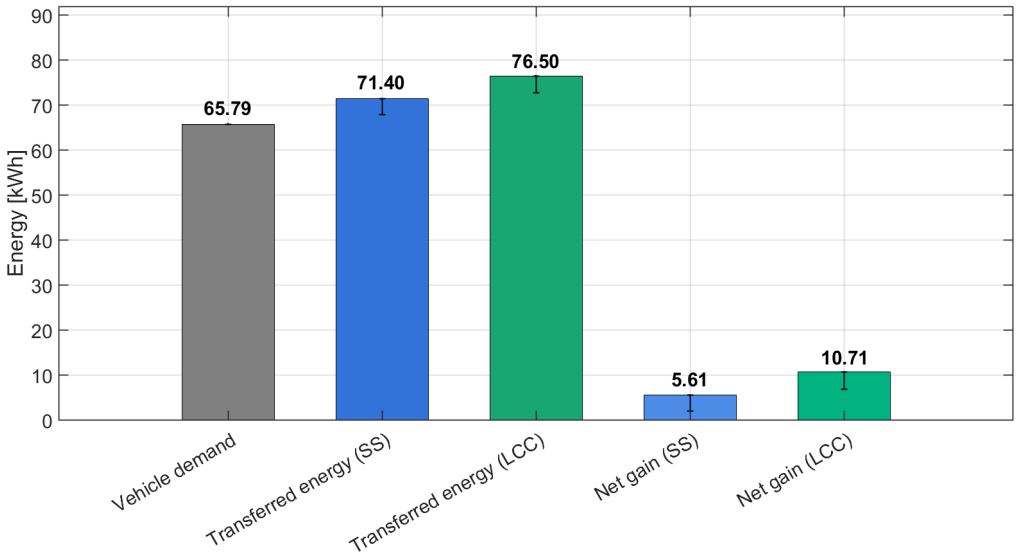


Figure 7. Net energy balance over the usable 510 km DWPT-equipped route, including variation ranges derived from moderate coupling fluctuations around the nominal operating condition.

While Figure 6 provides the most immediate vehicle-level interpretation of the two charging solutions through final SOC comparison, Figure 7 complements this view by explicitly separating vehicle energy demand, transferred energy, and net charging contribution over the usable electrified route. If studied together, these two figures help link the electrical comparison of the compensation topologies to their practical charging significance at vehicle level. The final SOC values were computed from the net energy balance over the usable 510 km DWPT-equipped roadway, considering a battery capacity of 75 kWh, a vehicle energy demand of 0.129 kWh/km, and the transferred-energy values obtained for the two investigated topologies. Under these assumptions, the final SOC reached 37.48% when the DWPT system operated with the SS compensation topology, and 44.28% when the LCC topology was adopted. In this case study, SOC evaluation is based on an energy balance formulation intended to provide a compact vehicle-level interpretation of DWPT effectiveness. Therefore, it does not explicitly include detailed battery charging constraints such as SOC-dependent charge acceptance, current-rate limitations, tapering behavior at higher SOC levels, battery-management-system actions, or thermal derating effects. In both cases, the final SOC is significantly higher than the initial one, which confirms that the transferred energy exceeds the vehicle consumption over the considered route. The difference between the two topologies is now more evident at vehicle level, since the higher transferred energy of the LCC topology results in a substantially larger SOC increase over distance. More specifically, the SOC increase is equal to 7.48 percentage points for the SS topology and 14.28 percentage points for the LCC topology. Overall, these results confirm that the proposed DWPT system can not only sustain vehicle operation but also provide a net battery recharge effect in both investigated configurations. The next section discusses these findings from a design-oriented perspective, with particular emphasis on the trade-off between simplicity, robustness, and energy transfer effectiveness in highway DWPT applications.

7. Discussion

The results presented in the previous section show that both compensation topologies are technically capable of enabling effective DWPT in the considered highway scenario. In both cases, the transferred energy per kilometer exceeds the benchmark vehicle consumption of 0.129 kWh/km, which means that the proposed infrastructure can provide

a net charging contribution during motion rather than merely slowing battery depletion. This finding is particularly relevant for long-distance electric mobility, since it confirms the potential of DWPT systems to support battery-electric vehicles on major highway corridors without requiring stationary charging events during the trip. It should also be noted that the present findings are derived under a constant-speed benchmark assumption. In real highway operation, speed fluctuations, acceleration and deceleration phases, lane changes, and congestion may alter the duration of the effective coupling intervals and the continuity of power transfer. Depending on the traffic condition, these effects may either reduce the average transferred energy, for example because of non-ideal alignment trajectories and intermittent coupling, or locally increase the residence time above active segments in low-speed conditions. Therefore, the SOC values reported in this study should be interpreted as benchmark estimates under controlled operating assumptions, rather than as fully traffic-resolved predictions. A first key outcome of the comparison concerns the different electrical behavior of the two compensation networks. The SS topology achieved the highest peak power, which is consistent with its strong dependence on favorable alignment conditions and instantaneous magnetic coupling, under the tuned resonant assumptions adopted in the present comparative model. For this reason, the SS topology appears well suited to applications in which high instantaneous transfer capability is desirable and system architecture simplicity is a priority. However, the present results also show that the highest peak power does not necessarily correspond to the best overall charging performance in a dynamic environment. Although the SS topology reached the larger maximum power, the LCC topology provided a higher average power and a greater transferred energy per kilometer. This aspect is particularly important for highway DWPT systems, because the vehicle continuously moves through regions of varying mutual inductance rather than remaining in a single optimal alignment condition. Under such circumstances, the capability to maintain a more regular transfer process over time becomes more valuable than isolated power maxima. From a physical and system-level perspective, the superior energy transfer performance of the LCC topology can be interpreted as a consequence of its higher robustness to coupling variations. In the considered scenario, the magnetic interaction between road-side and vehicle-side coils changes continuously as the vehicle progresses along the segmented charging track. A topology that is less sensitive to these variations can exploit a wider portion of the interaction interval, thereby increasing the useful area under the power curve. Under this interpretation, lateral misalignment would be expected to penalize the SS topology more strongly than the LCC topology, since the SS response is more dependent on favorable instantaneous coupling conditions, whereas the LCC configuration maintains a more regular transfer behavior under degraded coupling. This explains why the LCC topology, despite its lower peak power, achieves the highest transferred energy and the best final SOC result. In this sense, the better stability attributed to the LCC topology should be interpreted quantitatively as a more regular power transfer behavior under coupling variation, which is already evidenced in the present study by its higher average power, higher cumulative transferred energy, improved SOC increase, and more favorable sensitivity trend under reduced-coupling conditions. To complement the nominal-condition comparison, an additional sensitivity analysis was carried out by introducing the normalized coupling-reduction factor α. This parameter allows the robustness of the SS and LCC topologies to be qualitatively compared under degraded coupling conditions, and Figure 8 illustrates the corresponding trend of transferred power as the coupling condition is progressively reduced. It should be noted, however, that this sensitivity analysis is introduced as a compact surrogate representation of coupling degradation and not as a full three-dimensional electromagnetic model. Therefore, while it is useful for comparing the relative robustness of the two compensation topologies, it does not explicitly

account for lateral offset, vertical displacement changes, or vehicle attitude variations. A more detailed geometric coupling formulation or 3D electromagnetic co-simulation would provide a more accurate description of these effects and represents a future extension of this study.

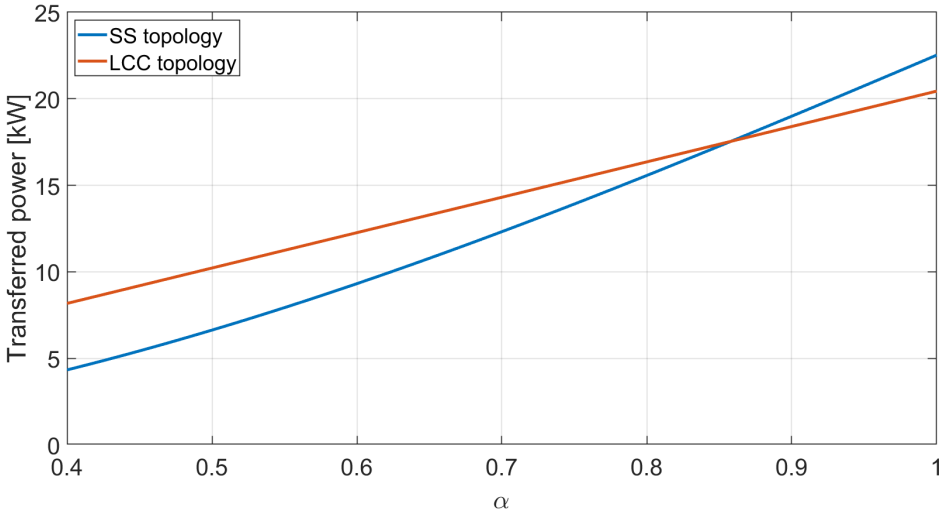


Figure 8. Sensitivity of transferred power to the normalized coupling-reduction factor α used to represent degraded coupling conditions associated with dynamic displacement and misalignment.

Accordingly, Figure 8 should be interpreted as a comparative robustness indicator rather than as a direct geometric tolerance map. In particular, the present sensitivity representation does not quantify separately the effects of lateral offset, vertical displacement, or coil-to-coil tolerance, but instead aggregates their impact into a single normalized coupling-reduction parameter. While this compact representation is useful for highlighting the relative behavior of the SS and LCC topologies, a more design-oriented analysis would require an explicit mapping between coupling degradation and physically measurable geometric deviations. These differences are not only relevant at the circuit-performance level, but also translate into a clearly distinguishable battery-support effect when the vehicle-level energy balance is evaluated over the full usable DWPT-equipped highway section. Starting from an initial SOC of 30%, the SS topology increases the SOC to 37.48%, whereas the LCC topology raises it to 44.28%. This confirms that the vehicle-level benefit of the LCC configuration is not marginal, but corresponds to a substantially greater net charging contribution during motion. This result has an important design implication in terms of engineering and application-oriented terms, namely with respect to compensation topology selection, charging continuity, transferred-energy effectiveness, and infrastructure-oriented DWPT design. While both topologies are capable of producing a meaningful charging effect, the superior transferred-energy performance of the LCC topology translates into a more pronounced battery-support outcome over long-distance highway operation. Therefore, the selection between the two topologies should not be based exclusively on peak-power capability, but should also account for the cumulative charging benefit delivered over distance, together with implementation complexity, component count, cost, control requirements, and expected operating robustness. In this regard, the two topologies can be seen as representing two different design philosophies for highway DWPT systems. The SS topology is attractive because of its simpler structure and lower circuit complexity, which may facilitate implementation and potentially reduce infrastructure cost. For this reason, the SS topology may remain a suitable option in application cases where simplicity, reduced component count, lower implementation burden, and high instantaneous power capability are prioritized over maximum cumulative energy transfer smoothness. This may include scenarios with

more controlled alignment conditions, reduced control-complexity requirements, or design contexts in which implementation robustness and architectural simplicity are considered more important than the highest vehicle-level charging gain. The LCC topology, by contrast, is more complex but offers a more stable electrical response, better current controllability, and a more uniform energy transfer process. At the same time, this practical advantage should be interpreted with some caution, since the current-source-like behavior of the LCC network is typically achieved only when suitable resonant operating conditions and converter control strategies are maintained. In real implementations, phase-shift control, resonant-frequency tracking, or equivalent control actions may be required to preserve stable operation under coupling variations. Therefore, the present comparison highlights the intrinsic energetic potential of the two topologies, while leaving the detailed control-design and control-robustness problem to future investigation. The present results also provide useful insight into the broader feasibility of highway DWPT deployment. At the same time, this feasibility assessment should be interpreted primarily in technical and energetic terms. A more holistic deployment evaluation would also require a techno-economic layer capable of accounting for coil installation density, power electronics architecture, infrastructure maintenance burden, and cost/performance trade-offs at corridor level. Since both investigated configurations yield an energy transfer greater than the benchmark vehicle consumption, the analyzed A4 case study appears favorable for the adoption of dynamic charging systems. Meanwhile, the present conclusions are derived from a single-vehicle benchmark framework. In large-scale highway deployment, multiple vehicles may simultaneously interact with the DWPT infrastructure, giving rise to shared segment activation, scheduling constraints, and infrastructure-management challenges that are not explicitly represented in the current model. For this reason, the present results should be interpreted as a topology-comparison benchmark rather than as a complete traffic-level deployment simulation. At the same time, some limitations of the present study should be explicitly acknowledged. First, the vehicle benchmark is based on a simplified constant-speed highway drive cycle and therefore does not fully capture real traffic variability, speed fluctuations, acceleration phases, or lane changes. Second, the analysis focuses on the energetic and topological comparison under fixed geometric assumptions, while additional aspects such as thermal effects, converter control, electromagnetic field compliance, infrastructure costs, and large-scale grid interaction were not explicitly modeled. More specifically, the present formulation does not include temperature-dependent coil resistance, inverter loss variation under dynamic loading, or environmental influences on continuous operation. Likewise, the present model does not provide a separate loss breakdown for winding copper losses, magnetic core and iron losses, or temperature rise in the compensation components. In real DWPT deployment, these effects may reduce the effective transferred power, modify the average energy delivered over distance, and influence component lifetime and reliability. Therefore, the reported energetic results should be interpreted as comparative benchmark estimates rather than as electro-thermally resolved performance predictions. Third, the comparison was carried out for one representative vehicle class and one specific roadway scenario; therefore, the conclusions should be interpreted as case study-based rather than universally generalizable. In addition, the vehicle-level SOC evolution was estimated through a simplified energy balance approach and does not yet reproduce the full dynamic charging behavior of a real traction battery. More realistic battery-side modeling would require the inclusion of SOC-dependent charge acceptance, BMS constraints, charging-power tapering, and thermal management effects. These limitations also point directly to future research directions. An additional limitation of the present work is the absence of experimental validation. The reported results are derived from simulation-based comparative modeling and should therefore be interpreted as benchmark indicators of relative

topology behavior rather than as prototype-validated performance predictions. In particular, no hardware-level measurements were included in this study to verify transferred power, efficiency, or stability under dynamic coupling variation, misalignment, and real operating conditions. A future extension of this work would be to introduce more realistic traffic and vehicle-dynamics conditions, including variable-speed drive cycles, acceleration and deceleration phases, lane-change events, congestion-dependent residence times, and misalignment distributions. Another important development would be the integration of a more detailed techno-economic analysis aimed at comparing the energetic benefits of the different compensation topologies with their installation density requirements, converter and compensation network complexity, maintenance burden, and infrastructure-level implementation costs. Finally, further work should investigate the scalability of the proposed DWPT system under multi-vehicle operation, including shared coil activation, scheduling logic, charging-priority management, and possible infrastructure-level interaction among simultaneous vehicles. Such an extension would make it possible to assess the operational feasibility of large-scale DWPT deployment under realistic highway traffic conditions, while also evaluating its interaction with the electrical grid in high-traffic environments. Moreover, the broader lifecycle implications of large-scale DWPT infrastructure, including material use, installation burden, maintenance requirements, and end-of-life considerations would be wortho of interest for future examinations. Overall, the discussion confirms that compensation topology selection plays a crucial role in the design of highway DWPT systems. The SS topology offers simplicity and high peak transfer capability, whereas the LCC topology provides better average performance and more stable energy delivery under dynamic operating conditions. For the A4 highway case study considered in this paper, both solutions prove feasible, but the LCC configuration emerges as the more favorable option when the primary design objective is to maximize effective transferred energy and charging continuity during motion.

8. Conclusions

This paper investigated the feasibility of a DWPT system for electric vehicle charging through a case study based on the Italian A4 highway. A segmented roadway-embedded charging architecture with planar circular coils was considered, and two compensation solutions, namely the SS and the LCC topologies, were comparatively assessed under the same vehicle, infrastructure, and magnetic coupling assumptions. The study was designed to connect topology-level electrical performance with vehicle-level charging effectiveness, using a benchmark battery electric vehicle traveling under highway conditions. The obtained results show that both topologies are capable of enabling effective dynamic charging in the selected scenario. In particular, the SS configuration achieved the highest peak power, equal to 22.52 kW, whereas the LCC topology provided the highest average power, equal to 13.47 kW, and the largest transferred energy, equal to 0.15 kWh/km. By comparison, the SS topology yielded an average power of 12.30 kW and a transferred energy of 0.14 kWh/km. Since both values exceed the benchmark vehicle demand of 0.129 kWh/km, the DWPT system was shown to provide not only support against battery depletion, but also a net charging contribution during motion. The vehicle-level analysis confirmed these findings. Starting from an initial state of charge (SOC) of 30%, the final SOC reached 37.48% with the SS topology and 44.28% with the LCC topology. These values confirm that both configurations provide a net charging contribution during motion, while also showing that the higher transferred energy of the LCC topology yields a substantially greater SOC increase over the usable 510 km electrified route. Accordingly, the LCC configuration offers the most favorable energetic behavior in the investigated highway application, owing to its more stable power transfer profile and greater robustness to coupling variations. Conversely, the SS

topology remains an attractive solution when circuit simplicity, reduced component count, and high instantaneous power capability are considered priority design factors. Overall, the study demonstrates that the A4 highway represents a promising application context for DWPT deployment and that compensation topology selection plays a central role in determining the balance between simplicity, robustness, and energy transfer effectiveness. Within the assumptions adopted in this work, the LCC topology emerges as the more advantageous option when the primary objective is to maximize useful transferred energy and charging continuity under dynamic conditions, while the SS topology offers a simpler alternative with strong peak-performance capability. Future developments should extend the present analysis by including more realistic traffic conditions, variable speed profiles, richer misalignment distributions, thermal constraints, converter control aspects, electromagnetic safety, and infrastructure-level economic considerations. In addition, further methodological refinement should address the adoption of more comprehensive geometric coupling models and 3D electromagnetic simulations capable of explicitly accounting for lateral offset, vertical displacement, and vehicle attitude variations during motion, in order to better assess the practical implementation trade-off between SS and LCC compensation. Further research may also address large-scale deployment issues, such as grid interaction, multi-vehicle operation, real case study deployment, and the integration of DWPT systems into broader electrified transport corridors. These developments would help strengthen the practical relevance of the present findings and support the transition from case study analysis to real-world implementation strategies.

Author Contributions: C.G.C.: Data Curation, Methodology, Software, Formal analysis, Conceptualization, Investigation, Writing—review and editing, Visualization; G.B.: Data Curation, Methodology, Software, Formal analysis, Investigation, Writing—original draft preparation, Visualization; M.L.: Writing—Review and Editing, Supervision, Project administration, Funding acquisition. All authors have read and agreed to the published version of the manuscript.

Funding: This research received no external funding.

Data Availability Statement: The original contributions presented in this study are included in the article. Further inquiries can be directed to the corresponding author.

Conflicts of Interest: The authors declare no conflicts of interest.

References

1. Jia, C.; Liu, W.; Chau, K.; He, H.; Zhou, J.; Niu, S. Passenger-aware reinforcement learning for efficient and robust energy management of fuel cell buses. *eTransportation* **2026**, *27*, 100537. [CrossRef]
2. de las Nieves Camacho, M.; Jurburg, D.; Tanco, M. Hydrogen fuel cell heavy-duty trucks: Review of main research topics. *Int. J. Hydrogen Energy* **2022**, *47*, 29505–29525. [CrossRef]
3. Wang, X.; Ji, J.; Li, J.; Zhao, Z.; Ni, H.; Zhu, Y. Review and Outlook of Fuel Cell Power Systems for Commercial Vehicles, Buses, and Heavy Trucks. *Sustainability* **2025**, *17*, 6170. [CrossRef]
4. Bi, Z.; Kan, T.; Mi, C.C.; Zhang, Y.; Zhao, Z.; Keoleian, G.A. A review of wireless power transfer for electric vehicles: Prospects to enhance sustainable mobility. *Appl. Energy* **2016**, *179*, 413–425. [CrossRef]
5. Machura, P.; Li, Q. A critical review on wireless charging for electric vehicles. *Renew. Sustain. Energy Rev.* **2019**, *104*, 209–234. [CrossRef]
6. Aydin, E.; Aydemir, M.T.; Aksoz, A.; El Baghdadi, M.; Hegazy, O. Inductive Power Transfer for Electric Vehicle Charging Applications: A Comprehensive Review. *Energies* **2022**, *15*, 4962. [CrossRef]
7. Rajamanickam, N.; Shanmugam, Y.; Jayaraman, R.; Petrov, J.; Vavra, L.; Gono, R. Review of Compensation Topologies Power Converters Coil Structure and Architectures for Dynamic Wireless Charging System for Electric Vehicle. *Energies* **2024**, *17*, 3858. [CrossRef]
8. Mi, C.C.; Buja, G.; Choi, S.Y.; Rim, C.T. Modern Advances in Wireless Power Transfer Systems for Roadway Powered Electric Vehicles. *IEEE Trans. Ind. Electron.* **2016**, *63*, 6533–6545. [CrossRef]

9. Xue, Z.; Liu, W.; Liu, C.; Chau, K.T. Critical Review of Wireless Charging Technologies for Electric Vehicles. *World Electr. Veh. J.* **2025**, *16*, 65. [CrossRef]
10. Apicella, V.; Turati, A.; Megna, G.; Carambia, B. Sizing Methodology of Dynamic Wireless Charging Infrastructures for Electric Vehicles in Highways: An Italian Case Study. *Energies* **2024**, *17*, 3922. [CrossRef]
11. Li, W.; Zhao, H.; Li, S.; Deng, J.; Kan, T.; Mi, C.C. Integrated *LCC* Compensation Topology for Wireless Charger in Electric and Plug-in Electric Vehicles. *IEEE Trans. Ind. Electron.* **2015**, *62*, 4215–4225. [CrossRef]
12. Li, S.; Li, W.; Deng, J.; Nguyen, T.D.; Mi, C.C. A Double-Sided LCC Compensation Network and Its Tuning Method for Wireless Power Transfer. *IEEE Trans. Veh. Technol.* **2015**, *64*, 2261–2273. [CrossRef]
13. Kan, T.; Nguyen, T.D.; White, J.C.; Malhan, R.K.; Mi, C.C. A New Integration Method for an Electric Vehicle Wireless Charging System Using LCC Compensation Topology: Analysis and Design. *IEEE Trans. Power Electron.* **2017**, *32*, 1638–1650. [CrossRef]
14. Mansour, H.S.; Samir, M.; Elhady, B.; Abdelmaksoud, S. Wireless charging systems for electric vehicles: Review. *Green Energy Intell. Transp.* **2026**, *5*, 100371. [CrossRef]
15. Deflorio, F.; Guglielmi, P.; Pinna, I.; Castello, L.; Marfull, S. Modeling and Analysis of Wireless "Charge While Driving" Operations for Fully Electric Vehicles. *Transp. Res. Procedia* **2015**, *5*, 161–174.. [CrossRef]
16. Colombo, C.G.; Ota, R.; Longo, M. Optimized Electric Vehicles Wireless Charging: Applicative Models for Supporting Decision Makers. *IEEE Open J. Veh. Technol.* **2025**, *6*, 897–911. [CrossRef]
17. Song, K.; Lan, Y.; Zhang, X.; Jiang, J.; Sun, C.; Yang, G.; Yang, F.; Lan, H. A Review on Interoperability of Wireless Charging Systems for Electric Vehicles. *Energies* **2023**, *16*, 1653. [CrossRef]
18. ElGhanam, E.; Hassan, M.; Osman, A. Design of a High Power, LCC-Compensated, Dynamic, Wireless Electric Vehicle Charging System with Improved Misalignment Tolerance. *Energies* **2021**, *14*, 885. [CrossRef]
19. Korakianitis, N.S.; Nikolaos, N.; Vokas, G.A.; Ioannidis, G.C.; Kaminaris, S.D. Simulation-Based evaluation of dynamic wireless charging systems for electric vehicles: Efficiency, limitations, and future directions. *AIMS Energy* **2025**, *13*, 590–631. [CrossRef]
20. The Mediterranean Corridor—Mobility and Transport—European Commission. Available online: https://transport.ec.europa.eu/transport-modes/rail/ertms/who-involved-ertms-deployment/corridors/mediterranean-corridor_en (accessed on 22 June 2026).
21. 'Volume del Traffico sui Tratti Elementari della rete Autostrade//per l'Italia-Anno 2014' (Edizione Aprile 2015). Available online: https://www.autostrade.it/documents/10279/0/SINTESI+volumi+2014.pdf/23516b4c-4a3f-4973-acfd-093c433e8f29 (accessed on 22 June 2026).
22. Budhia, M.; Covic, G.A.; Boys, J.T. Design and Optimization of Circular Magnetic Structures for Lumped Inductive Power Transfer Systems. *IEEE Trans. Power Electron.* **2011**, *26*, 3096–3108. [CrossRef]
23. Nagendra, G.R.; Covic, G.A.; Boys, J.T. Determining the Physical Size of Inductive Couplers for IPT EV Systems. *IEEE J. Emerg. Sel. Top. Power Electron.* **2014**, *2*, 571–583. [CrossRef]
24. Vishnuram, P.; Panchanathan, S.; Rajamanickam, N.; Krishnasamy, V.; Bajaj, M.; Piecha, M.; Blazek, V.; Prokop, L. Review of Wireless Charging System: Magnetic Materials, Coil Configurations, Challenges, and Future Perspectives. *Energies* **2023**, *16*, 4020. [CrossRef]
25. Covello, A.; Martino, A.D.; Longo, M. Experimental Observation and Validation of EV Model for Real Driving Behavior. *IEEE Access* **2024**, *12*, 130763–130776. [CrossRef]
26. Di Martino, A.; Martini, D.; Longo, M.; Zaninelli, D. Simulation of Electric Vehicle Energy Consumption of Real Driving Behaviour. In *Proceedings of the 2023 IEEE Vehicle Power and Propulsion Conference (VPPC)*; IEEE: New York, NY, USA, 2023; pp. 1–6. [CrossRef]
27. Di Martino, A.; Longo, M. Driving-Routine Variability of Energy Consumption for Electric Vehicle Through Virtual Reality. In *Proceedings of the 2025 International Conference on Intelligent Computing and Virtual & Augmented Reality Simulations (ICVARS)*; IEEE: New York, NY, USA, 2025; pp. 164–168. [CrossRef]
28. Wang, X.; Lu, C.; Wang, C.; Liu, P.; Xu, W.; Zhou, Y.; Wang, F. Methods for testing the performance of long-distance wireless power transmission systems. *EURASIP J. Wirel. Commun. Netw.* **2020**, *2020*, 251. [CrossRef]

Disclaimer/Publisher's Note: The statements, opinions and data contained in all publications are solely those of the individual author(s) and contributor(s) and not of MDPI and/or the editor(s). MDPI and/or the editor(s) disclaim responsibility for any injury to people or property resulting from any ideas, methods, instructions or products referred to in the content.